PHYSICAL REVIEW A VOLUME 39, NUMBER 3 FEBRUARY 1, 1989

Precision measurement of the $1s2s\ ^1S_0 - 1s2p\ ^1P_1$ interval in heliumlike beryllium

T. J. Scholl, R. A. Holt, and S. D. Rosner
Department of Physics, University of Western Ontario, London, Ontario, Canada N6A 3K7
(Received 8 September 1988)

Using fast-ion-beam laser spectroscopy, we have measured the $1s2s\ ^1S_0 - 1s2p\ ^1P_1$ interval in Be III to be 16 276.774(9) cm^{-1}. Frequency calibration was provided by an iodine absorption cell and the iodine atlas of Gerstenkorn and Luc [*Atlas du Spectre d'Absorption de la Molécule d'Iode: Partie III* (Editions du CNRS, Paris, 1978)]. This work represents an improvement in precision over previous measurements by an order of magnitude and is in excellent agreement with a very recent calculation of Drake [Can. J. Phys. **66**, 586 (1988)].

I. INTRODUCTION

Quantum electrodynamics (QED) is a highly successful fundamental theory of the interaction of charged particles with the quantized electromagnetic field. Because calculations with QED are extremely difficult and are carried out in a perturbative manner, it is important to compare theory with experiment in simple physical systems at the highest possible precision to test the methods of calculation and to look for possible breakdowns in the theory itself.

One of the most fruitful areas for such tests has been high-precision spectroscopy of one- and two-electron ions[1,2] spanning a wide range of atomic number Z. Hydrogenic ions have the attraction that there are bound states whose energy differences arise entirely from QED effects, and that these effects can be calculated to very high precision, especially for purely leptonic atoms. Direct resonance measurements of such intervals for $n=2$ in hydrogen and deuterium[3] provided the first quantitative evidence for the self-energy and vacuum polarization corrections to the Coulomb binding energy of an electron. Nevertheless, such measurements have serious linewidth limitations and are feasible at only a few values of Z because of the strong Z dependence of the transition frequencies. The only other technique that is capable of precision comparable to a resonance measurement is the quenching anisotropy method,[4] which is free of the linewidth limitation, but requires large systematic corrections and has not yet been widely applied.

Two-electron atoms present two apparent difficulties: The calculation of nonrelativistic energies and relativistic and QED corrections is much more difficult than in the one-electron case because of electron correlations, and the QED effects occur as a relatively small contribution to energy intervals dominated by nonrelativistic Coulomb effects. In the last decade, there has been remarkable progress on the theoretical side with much improved calculations of the nonrelativistic energy[1,5] and the Bethe-logarithm contribution to the self-energy.[6] The nonrelativistic energy can now be computed to parts in 10^{13}, even in the lightest ions, for which correlation effects are most significant. Current theoretical precision of a few ppm is limited by our knowledge of relativistic contributions of $O(\alpha^4 Z^4)$ now being computed. There is no doubt that further improvement is possible which will enable the most stringent tests of the theory with two-electron atoms.

On the experimental side, it was recognized some years ago that the $1s2s-1s2p$ transitions in heliumlike ions have especially attractive properties for the following reasons.

(i) The transition frequency increases slowly with Z ($\sim Z$); thus the wavelengths of light required for resonance measurements for $Z \leq 10$ are available from narrow-band coherent sources.

(ii) The transitions from the $1s2p\ ^3P_J$ levels to the ground state are suppressed by electric dipole and LS coupling selection rules, leading to natural linewidths for the $1s2s\ ^3S-1s2p\ ^3P$ transitions which are much smaller than those of hydrogenic Lamb-shift transitions and which scale approximately as Z.

(iii) The *relative* contribution to the total energy of relativistic and QED effects grows rapidly with Z ($\sim Z^3$).

(iv) As in hydrogenic ions, the lower level of the transition is metastable, allowing clean, low-background measurements with mass-selected beams.

There is therefore a range of heliumlike ions where the wavelengths involved permit spectroscopic measurements of high precision on transitions with significant relativistic and QED contributions. In fact the ratio of the QED portion to the experimental linewidth is actually *better* than for the hydrogenic $n=2$ Lamb shift. In the case of the $1s2s\ ^3S-1s2p\ ^3P$ intervals in Li II, where laser spectroscopy has been used,[7,8] this ratio is ~ 350, as compared with ~ 10 in hydrogen.

The work reported here is part of an ongoing project to make high-precision measurements of $1s2s\ ^3S-1s2p\ ^3P$ and $1s2s\ ^1S-1s2p\ ^1P$ intervals in low-Z heliumlike ions using laser spectroscopy. We have observed the $1s2s\ ^1S-1s2p\ ^1P$ transition in Be III at 614 nm and measured its energy to 0.5 ppm using I_2 absorption lines as an absolute reference. Previous measurements[9,10] (see Table I) using photographic spectrometry were at the

TABLE I. The $1s2p\ ^1P-1s2s\ ^1S$ interval in Be III (in cm^{-1}). The values in parentheses represent one-standard-deviation errors.

Experiment	Edlén[a]	16 279.0
	Löfstrand[b]	16 276.8(1)
	This work	16 276.774(9)
Theory	Drake[c]	16 276.766(20)

[a]Reference 9.
[b]Reference 10.
[c]Reference 5.

10-ppm level and appear to disagree with each other (although the experimental uncertainty in Ref. 9 can only be inferred).

II. EXPERIMENT

Be ions were produced from the metal using an oscillating electron bombardment ion source (see Fig. 1) similar in conception to the one used in our Li II measurements.[11] The major difference in design was to make the source much more compact and enclosed in order to achieve efficient high-temperature operation. Run times of over 10 h on a single fill were achieved, and the consumption of the highly toxic Be metal was reduced to a minimum. No support gas was needed to run the source. The typical anode current was 50 mA with an anode potential of 680 V relative to the cathode and anticathode.

The ion beam was extracted at ~ 10 kV, focused, and mass analyzed using a Wien filter. After further focusing, the beam was bent through an angle of 5° to make it collinear with the laser beam (see Fig. 2). To allow empirical elimination of the Doppler shift by the method introduced in Ref. 7, the laser beam was externally retroreflected so that two separate resonances could be observed, i.e., with the ion beam and laser beam *parallel* (*P*) and *antiparallel* (*A*). The ions were Doppler shifted into resonance with one of the laser beams using a small post-acceleration region, and finally deflected into a beam dump. Typical analyzed Be^{2+} currents were a few nA, of

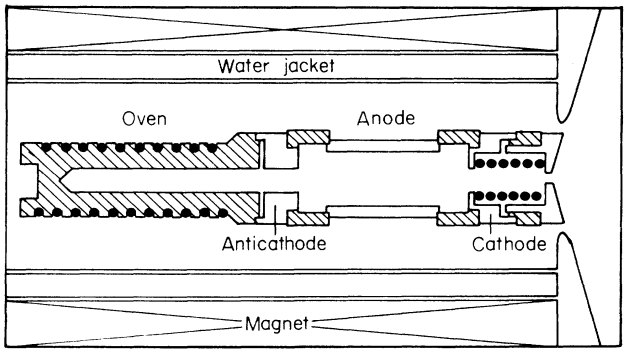

FIG. 1. Cross-sectional view of the oscillating electron bombardment ion source used to produce the Be^{2+} beam. The oven is loaded with several pieces of beryllium wire (not shown).

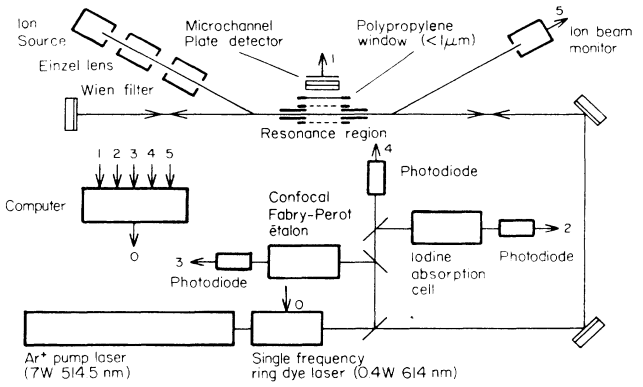

FIG. 2. Schematic layout of the experimental apparatus (not to scale). The ion beam travels from the source through the resonance region to the beam monitor in a vacuum of $< 10^{-7}$ Torr, and the laser beam enters and exits via Brewster windows (not shown) on both sides of the resonance region. The numbers 1–5 refer to detector signals input to the computer, while 0 refers to the computer-generated staircase ramp used to scan the laser.

which $\sim 3\%$ were in the $1s2s\ ^1S$ metastable state, as determined from the fluorescence intensity.

Any ions which absorbed a laser photon to reach the $1s2p\ ^1P$ state decayed primarily to the $1s^2\ ^1S$ ground state with the emission of a photon at 10.0 nm, which was detected by a two-stage microchannel plate (MCP) viewing the postaccelerator through a metallic mesh. It was vital to place a very thin (~ 1 μm) polypropylene window[12] in front of the detector in order to avoid a large background due to charged particles. With this window in place, the background was ~ 5 counts/s arising primarily from radiation generated by collisions of fast beam ions with a background gas of pressure $< 10^{-7}$ Torr. Typical signal levels were a few hundred counts per second.

The laser light was produced by a stabilized ring dye laser using Kiton red S dye pumped by ~ 7 W of 514.5-nm light from an argon-ion laser. The single-mode power in the interaction region was ~ 300 mW. Portions of the laser beam were picked off and directed to an I_2 absorption cell and a low-finesse Fabry-Pérot confocal étalon of 1 GHz free spectral range, for purposes of frequency calibration.

Under computer control, the laser was scanned in ~ 60-MHz steps over a range of 30 GHz with a dwell time of 0.25 s per step, while simultaneously recording the MCP counts, the transmitted laser power through the I_2 cell and étalon, the laser power, and the ion-beam current reaching the dump. Figure 3 shows typical data obtained in this way. A complete "run" consisted of a quartet of scans in a *PAAP* or *APPA* sequence. During this run, the ion-beam energy was left unchanged; comparison of the two *P* scans and two *A* scans provided a check on any drift of the ion-beam energy or geometry. Runs were made at a variety of ion-beam energies in the 8–10 keV/charge range to look for systematic effects

arising from the particular choice of I_2 calibration lines, changes in beam geometry, etc. The main constraint was to ensure that the two laser frequencies required for the P and A resonances coincided with regions of the I_2 spectrum known to contain a few well-characterized absorption lines.

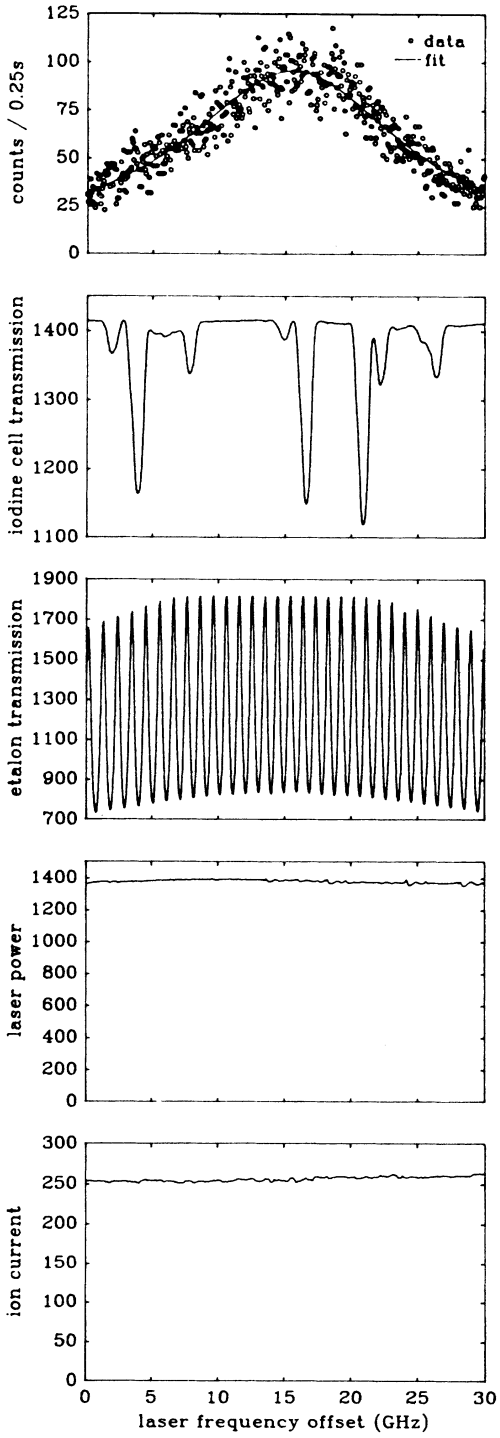

FIG. 3. Data collected in a single 30-GHz laser scan consisting of 512 steps of ~60 MHz with a duration of 0.25 s per step.

III. DATA ANALYSIS

In order to determine the center frequency of a given resonance signal, it was first necessary to convert the laser scan voltage (or channel number) to absolute frequency units. The Coherent 699-21 dye laser scan is controlled by means of a galvo-driven Brewster plate in its reference cavity. This leads to small (~2%) departures from linearity which vary smoothly over the scan range. We corrected for this with the aid of the 1-GHz étalon fringes. As a first step, each étalon transmission peak was separately fit with an Airy function[13] to determine its center in channel numbers. A polynomial fit of these centers to peak number produced a scale truly linear in frequency, but in arbitrary units. Finally, the scale was fixed absolutely using a few I_2 absorption lines whose frequencies were known from the I_2 atlas of Gerstenkorn and Luc.[14] Because the I_2 lines were noticeably asymmetric (due to hyperfine structure), their peak locations are not simply related to the values tabulated in the I_2 atlas. Following Gerstenkorn and Luc,[15] we performed a double convolution of the observed I_2 absorption spectrum to make it match the spectrum we would have obtained under the experimental conditions used for the atlas. This convolution procedure has been demonstrated to symmetrize the lines to the point where the difference between the peak and centroid values is negligible. A linear fit of the peaks of the convolved I_2 lines to their atlas frequencies completed the absolute frequency calibration. The error in this calibration was entirely negligible compared to the error in locating the resonance-signal line center.

Two corrections to the resonance signal are necessary to account for the effects of variations of laser power and ion-beam current over the 30-GHz laser scan. With careful adjustment, the laser power can be made to remain constant to within a few percent over the scan. The ion-beam current varies in a less predictable way, but can be remarkably stable over short periods. To guard against sudden changes, the computer software was written so as to halt data acquisition if the ion current varied beyond a chosen range. The resonance signals were normalized to both ion current and laser power to remove the effects of the remaining small variations in these quantities. The linearity of the signal with laser power was demonstrated by an experimental check in which the laser power was halved, and by theoretical modeling using the parameters of laser power, atomic lifetime, and interaction time relevant to this experiment.

Since the linewidth of the transition is dominated by the very short 8-ps lifetime[16] of the $1s2p\ ^1P$ state, the line shape should be well fit by a Lorentzian with a full width at half maximum (FWHM) of 19.4 GHz. However, we must give careful consideration to any effects which can produce even a slight asymmetry. One of these is the very small hyperfine structure of the $1s2p\ ^1P$ level. A detailed calculation in the Appendix shows that this leads to a shift of -3.0 MHz, which is entirely negligible at our level of precision.

A second effect, which was in fact experimentally observed, was a small asymmetry due to the Doppler effect.

However, in contrast to the hyperfine effect, this asymmetry *reverses exactly* in going from P to A geometry, and cannot affect the calculated Doppler-free line center which we extract from a run. The Doppler profile arising from the ion source conditions can be measured by observing spectral lines of other ions where natural broadening is negligible, and by using a viewing geometry which "sees" ions only in a relatively homogeneous region of the postaccelerator. The result implies a Doppler profile of FWHM ~ 150 MHz in 10-kV Be^{2+}, which makes a negligible contribution to the overall profile when convolved with a 19.4-GHz-wide Lorentzian.

The dominant source of Doppler broadening is the variation of electric potential in the postacceleration region viewed by the MCP. A study of the equipotentials and geometry of this region shows that the natural line profile should be convolved with an asymmetric profile with a FWHM of ~ 3 GHz. This profile is uncertain because it depends on the behavior of the MCP quantum efficiency as a function of angle, which must be extrapolated from published data.[17] In practice, we find that, with the signal-to-noise ratio present in a single spectrum, the asymmetry is not evident, and a good fit is obtained with a pure Lorentzian profile with a FWHM of $\sim 22.5(1.5)$ GHz, just barely statistically larger than the theoretical value. When many P or A spectra are superimposed by computer, the asymmetry shows up clearly and is indeed *reversed* between P and A spectra as expected (see Fig. 4). Defining the asymmetry α as the right HWHM minus the left HWHM divided by the FWHM, we find $\alpha(P) = -8.0(5)\%$ and $\alpha(A) = 8.3(5)\%$. In view of the smallness of the asymmetry and the cancellation between P and A spectra mentioned above, we are confident that the effect of line asymmetry on the final Doppler-free result is insignificant within the error quoted. The mean FWHM is consistent with theory but can only be used to set an upper limit on the decay rate because of the aforementioned uncertainty in MCP efficiency.

The frequency ν_0 of the transition in the ion rest frame is related to the observed laboratory P and A frequencies ν_p and ν_a by the relativistic Doppler formula,

$$\nu_0 = \gamma(1-\beta)\nu_p = \gamma(1+\beta)\nu_a \ ,$$

where β and γ have their usual definitions. Solving these for ν_0 gives

$$\nu_0 = \sqrt{\nu_p \nu_a} \ .$$

For a given run, the average of the two P scans and the average of the two A scans were used to compute ν_0, thus effectively eliminating the Doppler shift to all orders. A histogram showing the results of 30 runs is presented in Fig. 5, while Table I compares our final result with other work. The dominant contributions to the uncertainty are drifts in the beam energy, which appear to be quasirandom over many runs, and shot noise in the photon counting. If the two ν_p or ν_a values for a given run reveal a drift which is large compared to their statistical error, the run is rejected. The overall mean value of ν_0 is not sensitive within its quoted error to the precise criterion for such rejection. Systematic effects such as thermal drift of the calibration étalon and accuracy of the I_2 atlas are negligible compared to the quoted precision. Figure 6 shows ν_0 as a function of ion-beam energy per unit charge. Although some clustering of values of ν_0 at a given energy is evident, the randomness of the overall dis-

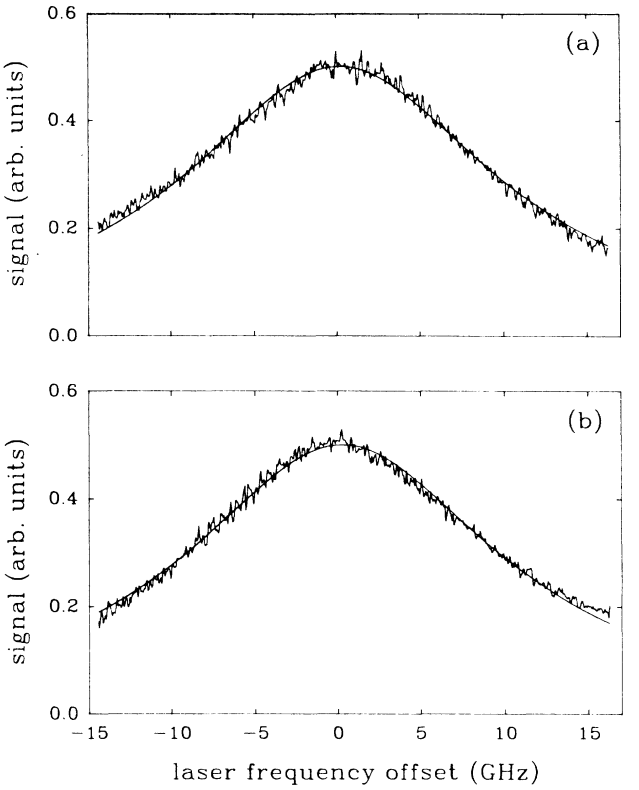

FIG. 4. Summed data from all scans in the (a) parallel and (b) antiparallel laser-beam–ion-beam configurations, together with the best-fit *symmetric* Lorentzian functions in order to display the small asymmetry in the line profiles.

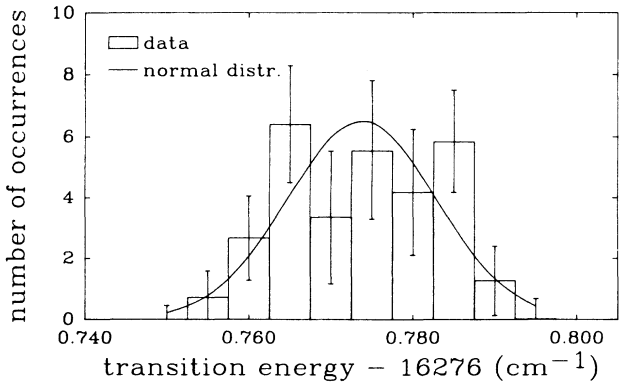

FIG. 5. Histogram showing the distribution of Doppler-free transition wave numbers for all of the data (30 runs).

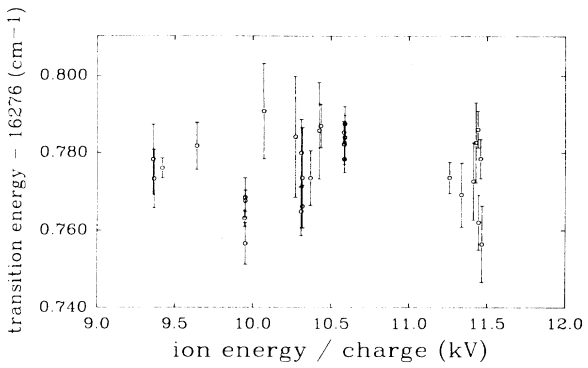

FIG. 6. Graph of transition wave number vs ion-beam energy per unit charge to illustrate the lack of systematic trends.

tribution indicates that residual systematic effects due to varying ion source conditions can be averaged out with many runs. We can find no evidence for a systematic beam-energy dependence of the measured ν_0.

IV. CONCLUSIONS

We have measured the $1s2s\ ^1S-1s2p\ ^1P$ interval in Be III to an accuracy of 0.5 ppm using fast-ion-beam laser spectroscopy. The result is in excellent agreement with theory and with the earlier result of Löfstrand,[10] with an improvement in precision by a factor of 11. It is clear that a laser measurement of the $1s2s\ ^3S-1s2p\ ^3P_J$ intervals can reach much greater precision because of the much narrower linewidth; the ultimate linewidth limit is 5.4 MHz, due to the 29-ns lifetime of the $1s2p\ ^3P_J$ levels. In the present experiment, an improved design for the post-accelerator and viewing geometry would substantially eliminate any Doppler broadening and yield a $\sim 5\%$ measurement of the $1s2p\ ^1P$ decay rate.

The increasing availability of intense, narrow-band uv light sources and novel ion sources should allow high-precision measurements of this type to be extended to the region of $Z\sim 10$. With the ongoing development of improved theoretical methods for two-electron atoms, highly significant comparisons can be made which may provide the best tests of QED for some time to come.

ACKNOWLEDGMENTS

We thank Professor Gordon Drake for sharing results prior to publication, and Professor Pedro Goldman for many helpful conversations. We are indebted to Steven Leffler for computational help in the data analysis. We gratefully acknowledge the support of the Natural Science and Engineering Research Council of Canada for this work.

APPENDIX: EFFECT OF HYPERFINE STRUCTURE OF THE $1s2p\ ^1P_1$ STATE ON THE OBSERVED LINE PROFILE

The presence of unresolved hyperfine structure (hfs) in the $1s2s\ ^1S_0-1s2p\ ^1P_1$ transition can in principle alter the line profile and shift the centroid. Since the total electronic angular momentum J of the metastable $1s2s\ ^1S_0$ level is zero, we need consider only the hyperfine structure of the $1s2p\ ^1P_1$ state. The $I=\frac{3}{2}$ nuclear spin of ^{9}Be produces three hyperfine components with total angular momentum $F=\frac{5}{2}$, $\frac{3}{2}$, and $\frac{1}{2}$. The magnetic interactions of the electrons with the nuclear magnetic dipole can be written as $\mathcal{H}_{\rm hfs}=A(J)\mathbf{I}\cdot\mathbf{J}$, which has the property that the centroid of three hyperfine sublevels remains unshifted, i.e., $\sum_F(2F+1)\langle\mathcal{H}_{\rm hfs}\rangle_F=0$. This implies that, if the intensities of the three hyperfine components of the fluorescence are proportional to $2F+1$, there will be no shift of the centroid of the fluorescence line profile. In this appendix we estimate the size of the hfs and the resulting effect on the centroid.

We begin by noting that the *fine-structure* interaction mixes the $1s2p\ ^1P_1$ and $1s2p\ ^3P_1$ states, so that we must calculate the hfs of the state,[16]

$$|\psi\rangle\equiv\cos\theta|1s2p\ ^1P_1\rangle-\sin\theta|1s2p\ ^3P_1\rangle\ ,$$

where $\sqrt{2}\tan\theta=2.4106\times10^{-3}$. The hyperfine energies are then given by

$$\begin{aligned}\Delta E_{\rm hfs}&=\langle\psi|\mathcal{H}_{\rm hfs}|\psi\rangle\\&=\cos^2\theta\langle 1s2p\ ^1P_1|\mathcal{H}_{\rm hfs}|1s2p\ ^1P_1\rangle\\&\quad-2\sin\theta\cos\theta\langle 1s2p\ ^3P_1|\mathcal{H}_{\rm hfs}|1s2p\ ^1P_1\rangle\\&\quad+\sin^2\theta\langle 1s2p\ ^3P_1|\mathcal{H}_{\rm hfs}|1s2p\ ^3P_1\rangle\ ,\end{aligned}$$

where, in the nonrelativistic approximation, the magnetic dipole hfs interaction can be written as[18]

$$\mathcal{H}_{\rm hfs}=\mathcal{H}_{\rm orb}+\mathcal{H}_{dd}+\mathcal{H}_{\rm FC}\ ,$$

with

$$\mathcal{H}_{\rm orb}=K\mathbf{I}\cdot\sum_i\frac{\boldsymbol{l}_i}{r_i^3}\ ,$$

$$\mathcal{H}_{dd}=-K\mathbf{I}\cdot\sum_i\frac{1}{r_i^3}\left[\mathbf{s}_i-\frac{3(\mathbf{s}_i\cdot\mathbf{r}_i)\mathbf{r}_i}{r_i^2}\right]\ ,$$

$$\mathcal{H}_{\rm FC}=K\mathbf{I}\cdot\sum_i^1\frac{8\pi}{3}|\varphi_i(0)|^2\mathbf{s}_i\ ,$$

and

$$K\equiv\left[\frac{\mu_0}{4\pi}\right]\left[\frac{2\mu_B\mu_I}{I}\right]\ .$$

Here $\boldsymbol{l}_i$, $\mathbf{s}_i$, $\mathbf{r}_i$, and φ_i are, respectively, the orbital angular momentum, spin, position, and wave function of the ith electron, μ_B and μ_I are the Bohr magneton and nuclear magnetic moment, and $\mathcal{H}_{\rm orb}$, $\mathcal{H}_{dd}$, and $\mathcal{H}_{\rm FC}$ represent the orbital, dipole-dipole, and Fermi-contact hfs interactions.

Because of the very small value of $\sin^2\theta$, we need consider only the terms in $\cos^2\theta$ and $\sin\theta\cos\theta$. There are thus three diagonal and three off-diagonal matrix elements to evaluate for $\langle\psi|\mathcal{H}_{\rm hfs}|\psi\rangle$. The diagonal matrix elements of $\mathcal{H}_{dd}$ and $\mathcal{H}_{\rm FC}$ vanish for the $1s2p\ ^1P_1$ state, since the expectation value of $\mathbf{s}_i$ in a spin singlet state is zero. Thus the only diagonal contribution is given by

$$\langle 1s2p\ ^1P_1,F|\mathcal{H}_{\rm orb}|1s2p\ ^1P_1,F\rangle = K\langle r^{-3}\rangle_{2p}\tfrac{1}{2}[F(F+1)-J(J+1)-I(I+1)]\ .$$

A reasonable estimate for $\langle r^{-3}\rangle_{2p}$ can be obtained from the hydrogenic result for a nuclear charge $Z_{\rm eff}=Z-1$ to take account of screening by the $1s$ electron:

$$\langle r^{-3}\rangle_{nl}=\frac{1}{l(l+\frac{1}{2})(l+1)n^3}\left[\frac{Z_{\rm eff}}{a_0}\right]^3 .$$

Numerical results for

$$\Delta E_{\rm orb}\equiv\cos^2\theta\langle 1s2p\ ^1P_1|\mathcal{H}_{\rm orb}|1s2p\ ^1P_1\rangle$$

are given in Table II.

Because the off-diagonal matrix elements are multiplied by $\sin\theta$, we need consider only the one involving $\mathcal{H}_{\rm FC}$, which is typically the largest interaction when it does not vanish identically. Using standard angular momentum algebra, one can show that

TABLE II. Calculated hyperfine structure $\Delta E_{\rm hfs}$ of the "$1s2p\ ^1P_1$" state $|\psi\rangle$, including orbital and Fermi contact contributions $\Delta E_{\rm orb}$ and $\Delta E_{\rm FC}$.

F	$\Delta E_{\rm orb}$ (MHz)	$\Delta E_{\rm FC}$ (MHz)	$\Delta E_{\rm hfs}$ (MHz)
$\frac{5}{2}$	−126.4	23.1	−103.3
$\frac{3}{2}$	84.3	−15.4	68.9
$\frac{1}{2}$	210.7	−38.5	172.2

$$\langle 1s2p\ LSJIFM_F|\mathbf{s}_1\delta^3(\mathbf{r}_1)+\mathbf{s}_2\delta^3(\mathbf{r}_2)|1s2p\ L'S'J'I'F'M'_F\rangle = \delta_{FF'}\delta_{M_FM'_F}\delta_{II'}\delta_{LL'}(-1)^{F+I+J'+2S'+J+L+1}\left[\frac{I(I+1)(2I+1)3(2J+1)(2J'+1)3(2S+1)(2S'+1)}{6(2L+1)}\right]^{1/2} \times\begin{Bmatrix}J & 1 & J'\\ I' & F & I\end{Bmatrix}\begin{Bmatrix}J' & S' & L\\ S & J & 1\end{Bmatrix}\begin{Bmatrix}s & 1 & s'_2\\ S' & s_1 & S\end{Bmatrix}\langle 1s2p\ L\|\delta^3(\mathbf{r}_1)\|1s2p\ L'\rangle\ ,$$

where the subscript 1 refers to the $1s$ electron. The reduced matrix element involving the Dirac δ function can be written in terms of $\langle\delta^3(\mathbf{r}_1)\rangle_{1s}$ using the Wigner-Eckart theorem and then evaluated using hydrogenic wave functions to give

$$\langle 1s2p\ L=1\|\delta^3(\mathbf{r}_1)\|1s2p\ L=1\rangle=\sqrt{3}\frac{Z^3}{\pi a_0^3 n^3}\ ,$$

with $Z=4$ and $n=1$. This contribution $\Delta E_{\rm FC}\equiv-2\sin\theta\cos\theta\langle 1s2p^3P_1|\mathcal{H}_{\rm FC}|1s2p\ ^1P_1\rangle$ is given in Table II along with the total hfs $\Delta E_{\rm hfs}$.

The relative intensities of the three hyperfine components of the fluorescence from the $1s2p\ ^1P_1$ state to the $1s^2\ ^1S_0$ ground state can be calculated in two steps. First, making the assumption of uniform population of all $1s2s\ ^1S_0$ $F=\frac{1}{2}$ magnetic sublevels, we can calculate the relative populations $P(F,M)$ of the $1s2p\ ^1P_1$ sublevels for excitation by a laser linearly polarized along the z axis:

$$P(F,M)\propto|\langle 1s2p\ L'SIJ'F'M'|z|1s2s\ LSIJFM\rangle|^2 \propto(2F+1)(2F'+1)\times\begin{pmatrix}F' & 1 & F\\ -M' & 0 & M\end{pmatrix}^2\begin{Bmatrix}J' & 1 & J\\ F & I & F'\end{Bmatrix}^2\delta_{MM'}\ .$$

The fluorescence is viewed by a detector with a solid angle of 0.26 sr centered around an axis perpendicular to the z axis. For transitions with $\Delta M=0$, the intensity varies as $\sin^2\theta$, while for transitions with $\Delta M=\pm1$, the intensity varies as $\frac{1}{2}(1+\cos^2\theta)$, where θ is the angle between the line-of-sight and the z axis. These functions are then integrated over the solid angle subtended by the detector. The intensity $I(F',M',F,M)$ of a given fluorescence transition is given by

$$I(F',M',F,M)\propto(2F+1)(2F'+1)\times\begin{pmatrix}F & 1 & F'\\ -M & \Delta M & M'\end{pmatrix}^2\begin{Bmatrix}J & 1 & J'\\ F' & I & F\end{Bmatrix}^2 .$$

Combining these factors we arrive at the relative intensities $W(F)$ of observed fluorescence from each hyperfine level of the $1s2p\ ^1P_1$ state. With the normalization $\sum_F W(F)=1$, we have $W(F)=0.5070$: 0.3437: 0.1493 for the $F=\frac{5}{2}$, $\frac{3}{2}$, and $\frac{1}{2}$ levels, respectively.

With the $W(F)$ as the weights, the centroid $\sum_F W(F)\Delta E_{\rm hfs}(F)=-3.0$ MHz. A fit of a single Lorentzian to the sum of three Lorentzian curves centered at the calculated hyperfine energies with amplitudes proportional to $W(F)$ yields a frequency shift of −3.0 MHz as expected and a line broadening of 3.0 MHz. Both of these effects are entirely negligible at the present level of precision.

[1]G. W. F. Drake, Can. J. Phys. **66**, 586 (1988).
[2]G. W. F. Drake, Adv. At. Mol. Phys. **18**, 399 (1982).
[3]S. Triebwasser, E. S. Dayhoff, and W. E. Lamb, Jr., Phys. Rev. **89**, 98 (1953).
[4]G. W. F. Drake, J. Patel, and A. van Wijngaarden, Phys. Rev. Lett. **60**, 1002 (1988).
[5]G. W. F. Drake, Nucl. Instrum. Methods B **31**, 7 (1988).
[6]S. P. Goldman and G. W. F. Drake, J. Phys. B **17**, L197 (1984).
[7]R. A. Holt, S. D. Rosner, T. D. Gaily, and A. G. Adam, Phys. Rev. A **22**, 1563 (1980).
[8]E. Riis, H. G. Berry, O. Poulsen, S. A. Lee, and S. Y. Tang, Phys. Rev. A **33**, 3023 (1986).
[9]B. Edlén, Ark. Fys. **28**, 441 (1951).
[10]B. Löfstrand, Phys. Scr. **8**, 57 (1973).
[11]R. A. Holt, S. D. Rosner, T. D. Gaily, and A. G. Adam, Rev. Sci. Instrum. **52**, 157 (1981).
[12]A. J. Caruso and H. H. Kim, Rev. Sci. Instrum. **39**, 1059 (1968).
[13]M. Born and E. Wolf, *Principles of Optics,* 6th ed. (Pergamon, Oxford, 1980).
[14]S. Gerstenkorn and P. Luc, *Atlas du Spectre d'Absorption de la Molécule d'Iode: Partie III,* and *Complément: Identification des Transitions du Système B-X* (Editions du CNRS, Paris, 1978).
[15]S. Gerstenkorn and P. Luc, Rev. Phys. Appl. **14**, 791 (1979).
[16]G. W. F. Drake, Phys. Rev. A **19**, 1387 (1978).
[17]W. Parkes, R. Gott, and K. A. Pounds, IEEE Trans. Nucl. Sci. **NS-17**, 360 (1970).
[18]G. K. Woodgate, *Elementary Atomic Structure,* 2nd ed. (Oxford University Press, Oxford, England, 1980).